PHILOSOPHICAL TRANSACTIONS OF THE ROYAL SOCIETY A MATHEMATICAL, PHYSICAL & ENGINEERING SCIENCES

Picosecond Spectroscopic Studies of Biological Systems

P. M. Rentzepis

Phil. Trans. R. Soc. Lond. A 1979 **293**, 455-468
doi: 10.1098/rsta.1979.0112

Phil. Trans. R. Soc. Lond. A **293**, 455–468 (1979)
Printed in Great Britain

Picosecond spectroscopic studies of biological systems

By P. M. Rentzepis
Bell Laboratories, Murray Hill, New Jersey 07974, *U.S.A.*

Picosecond spectroscopy has been utilized to study ultrafast molecular processes occurring on a picosecond time scale. The experimental system for generating the excitation pulse and the probing picosecond continuum is described. The detection system and the advantages of employing a double-beam picosecond spectrometer with a computerized three dimensional display are presented. A study of the primary events in rhodopsin from 300 to 4 K is presented in some detail.

Introduction

As a result of the development of mode-locked laser technology, time-resolved spectroscopy can now be performed with picosecond (10^{-12} s = 1 ps) resolution. The ability to perform spectroscopic measurements on this time scale has produced in recent years a wealth of new information about ultrafast processes in physical and chemical systems (Eisenthal 1975; Kaufman & Rentzepis 1975; Lauberau & Kaiser 1975; Alfano & Shapiro 1975; Huppert & Rentzepis 1976). A range of phenomena has been studied utilizing picosecond time-resolved spectroscopy, including vibrational relaxation, radiationless electronic transitions, molecular orientational relaxation in solutions, excess electron trapping and solvation, fast processes in laser dyes, cage effects in solution, proton transfer reactions, and primary events in photobiology. Although the principal emphasis of the present paper centres on the characteristics and capabilities of many of the techniques employed in picosecond spectroscopy, the power of the method is illustrated in its application to the study of the intermediate steps in the visual transduction process reflected by the photoinduced changes in rhodopsin, the visual chromophore. Picosecond kinetics from room temperature to that of liquid helium reveal that a new mechanism, proton tunnelling, is the primary event in rhodopsin, at least at low temperatures.

Experimental techniques

An experimental configuration for single-pulse picosecond spectroscopic studies, which embodies several of the latest advances, is shown in figure 1. The laser oscillator uses neodymium glass (lasing transition 1060 nm) as the gain medium. Mode-locking of the laser is achieved by placing into the cavity a cell containing a saturable absorbing dye, usually Kodak 9860, which has a fast recovery (*ca.* 7 ps) from the bleached state. The reduced absorption loss that is experienced by pulses with duration of the order of or shorter than this recovery time is responsible for the short pulses produced. The output of the laser consists of a train of about 100 pulses, each of which has a duration in the range 5–10 ps. The interpulse separation in the train is equal to the round trip transit time of light within the laser cavity (typically 5–10 ns).

Although most lasers can be mode-locked, the highest powers have been achieved with neodymium glass lasers, and these have therefore been used extensively for picosecond experiments. Aside from the mode-locked laser, numerous variations exist in the experimental

approach for obtaining picosecond time-resolved spectroscopic information (Kaufman & Rentzepis 1975; Alfano & Shapiro 1975; Huppert & Rentzepis 1976). The particular selection of techniques which we employ is by no means universal, and therefore we shall proceed systematically through the experimental configuration in figure 1, briefly describing the function and relative importance of each major component.

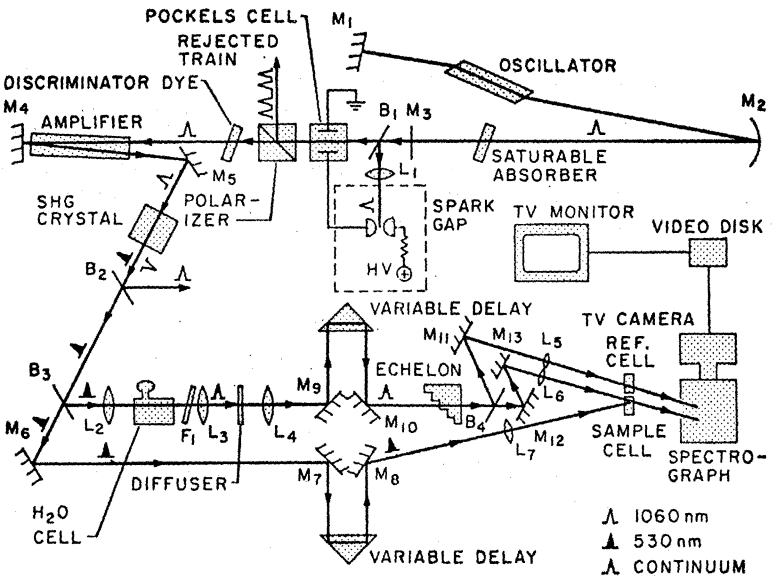

FIGURE 1. An experimental configuration used in picosecond absorption experiments. A single pulse is extracted by the Pockels cell and polarizer. After amplification a single second harmonic pulse (530 nm) is generated, part of which is split at B_3 to produce a continuum in the H_2O cell. The continuum pulse dispersed in time by the echelon is used to probe changes in the sample. Time-resolved spectra are recorded by TV camera and video disk. Mirrors, beamsplitters, lenses, and filters are designated by M, B, L, and F respectively.

Single pulse generator

The Pockels cell and polarizer in figure 1 are used to select a pulse from the mode-locked pulse train. We use single pulses in most experiments for several reasons. First, many processes being studied are either irreversible or have a decay component which is the order of or longer than the separation between pulses in the mode-locked train. In such cases the effect of *ca.* 100 pulses would be cumulative and thus would be complicated, if not impossible, to resolve. In addition, the properties of the pulses such as energy, time width, frequency width, and pulse substructure vary throughout the train (Glenn & Brienza 1967; von der Linde 1972). Thus a measurement of the experimental results for a single set of pulse parameters occurring with a single pulse is more meaningful than an ill-defined average over these parameters resulting from full-train measurements. Finally, with a single pulse, it is possible to achieve double-pass gains of *ca.* 100 in an optical amplifier. Gain saturation and/or optical component damage occur before gains of this magnitude are reached when the entire train is passed through the amplifier. It is frequently necessary to generate the highest possible intensities at 1060 nm for experiments especially in the u.v. region, and in these circumstances, large amplifier gains are required. A typical Nd^{3+} glass pulse shown in figure 2 (*a*) has a width of *ca.* 100 cm^{-1} (f.w.h.m.) and is characterized by the multispiked structure. Such large spectral width and nondescript structure is not suitable for most chemical studies where the transition bandwidth is narrower than *ca.* 200 cm^{-1}. To alleviate this problem we have devised (Huppert & Rentzepis 1978)

a means by which the oscillator pulse passes through a Nd/YAG amplifier resulting in 3 cm^{-1}, 6 ps pulse shown in figure 2 (*b*).

Frequency shifting techniques

The infrared 1060 nm pulses from the laser have found only limited direct usage in picosecond experiments. In most cases, the second harmonic frequency at 530 nm is produced by propagation of the infrared pulses through a second harmonic generating (s.h.g.) crystal such as KDP or $LiNbO_3$. Depending on the wavelength requirements of the experiment, additional frequency changes in the light may be achieved by repeated harmonic generation or nonlinear mixing to obtain the fourth harmonic at 265 nm or the third harmonic at 350 nm. Each consecutive harmonic generation step has an efficiency of 5–25%. In figure 1, only light of the second harmonic frequency is shown as generated.

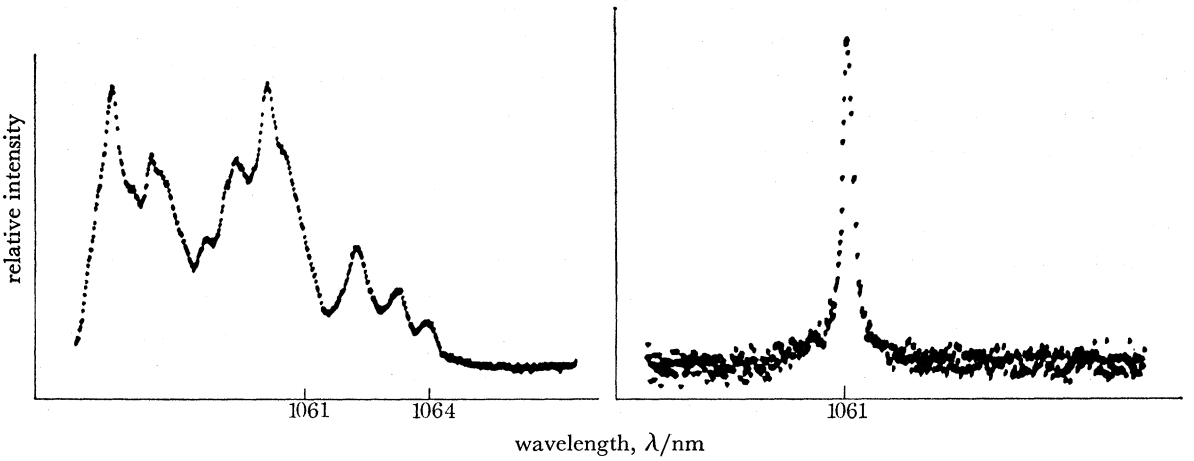

FIGURE 2. (*a*) Spectrum of single picosecond pulse emitted by the Nd^{3+}/silicate glass oscillator. The spectral structure varies within the pulses of a single train and from one shot to another. The average spectral width of Nd^{3+}/ED-2 silicate glass oscillator pulse is *ca.* 100 cm^{-1}. (*b*) Spectrum of Nd^{3+}/glass picosecond pulse amplified by Nd^{3+}/YAG. The right-hand peak corresponds to the well known Nd^{3+}/YAG laser line at 1064 nm. The centre peak is *ca.* 30 cm^{-1} shifted from the 1064 nm, i.e. *ca.* 1061 nm. The spectral width at half-maximum of each of these two lines is *ca.* 3 cm^{-1}.

Smaller frequency shifts may be achieved with high efficiency (*ca.* 10–60%) via stimulated Raman scattering processes. In this case the magnitude of the shift can be varied from 500 to 4000 cm^{-1} by selecting a molecule with the appropriate Raman transition frequency. When used in combination with harmonic generation, virtually the entire spectral region from near infrared to near ultraviolet is accessible to time-resolved picosecond studies at a coarse resolution of approximately 500 cm^{-1}. An additional frequency shifting technique which permits continuous resolution for absorption spectroscopy is discussed below, with the description of analysing probe techniques.

Time-resolved absorption techniques

After light of appropriate wavelength for the excitation process has been generated and filtered to remove other frequencies, a portion of it may be split off (at beamsplitter B_3 in figure 1) for use in the analysing beam. The remainder is propagated through a timing delay line (mirrors M_6–M_8) before exciting an area within the sample cell. The lens (L_7) reduces the cross-sectional area of the pulse, thereby increasing the power density at the excitation region.

In absorption spectroscopy experiments, the same region illuminated by the intense excitation pulse is probed by the analysing beam. The time between the arrival of the excitation and probe pulse at each wavelength is usually adjusted by some form of variable delay which does not change the experimental alignment, such as the translatable mirrors shown in figure 1 (Rentzepis 1968). The concentration of absorbing species present at the time of arrival of the probe pulse is then computed from I_0/I in the usual manner.

Time-resolved emission spectroscopy may also be performed with picosecond resolution. For these measurements time resolution is achieved by using the analysis pulse split from the excitation pulse to operate some form of ultrafast optical light gate. More recently, direct electronic picosecond resolution has been achieved with streak cameras (Bradley & Siebert 1973) and improvements continue to be made in this technique.

The remaining discussion of picosecond techniques pertains strictly to absorption spectroscopy, although the techniques are similar for applications involving emission measurements. In absorption, the analysing probe pulse may be used directly in the form in which it is split from the excitation pulse, or it may be further modified in wavelength and temporal characteristics during propagation along the optical path traversed by the analysing beam. The modifications typically imposed upon the probe pulse vary markedly in the experiments performed by different research groups and thus they represent a major point of departure in experimental approaches to the collection of time-resolved spectroscopic data.

Until recently, the majority of picosecond spectra were recorded in a point-by-point fashion, i.e. probe light of a single wavelength and at a particular time delay was recorded with one laser shot. Typically, the time dependence at a single wavelength was determined by moving the translatable mirrors or prism stage between laser shots, and occasionally such a set of time measurements was made at several wavelengths by using frequency-shifting techniques of the types described above.

Although numerous groups continue to use the pointwise approach because of its simplicity, in many of the experiments in our laboratories we have used dispersive methods in preference to frequency-shifting and time-delaying techniques. In the dispersive techniques the probe light pulse, which initially has narrow spectral and temporal widths, is spread out in one or both of these widths in an experimentally resolvable manner. With the strongly dispersive techniques currently employed, extended spectral and temporal regions are spanned by a single probe pulse and thus a complete time-resolved spectrum can be recorded with this single pulse. This capability not only reduces data collection times but also permits all of the data to be related to a pulse with a single set of optical properties, i.e. pulse width and power, frequency width, etc. The variation of these parameters with position of the pulse within a mode-locked train has already been mentioned but additional large variations occur for the properties of the single pulses selected from one laser shot to the next, making data gathered in a pointwise manner intrinsically more difficult to correlate with conditions of the excitation process. The techniques for generating the dispersion in wavelength and time are described briefly below.

Continuum generation

Much of the early work with high-power lasers involved studies of nonlinear interactions such as stimulated Raman scattering in liquids and solids (Colles 1969; Chiao & Stoicheff 1964) and self-broadening processes in liquids (Shimizu 1967, Gustafson *et al.* 1969), particularly liquids with high Kerr constants. In CS_2 it was observed (Shimizu 1967) that intense

laser lines could be broadened or dispersed to several hundred wavenumbers. Then in 1970 it was observed (Alfano & Shapiro 1970) that focusing intense picosecond pulses into many solids and liquids produced superbroadened continua, with widths greater then $10^4\,\mathrm{cm}^{-1}$. When it was shown (Busch *et al.* 1973) that these continua also had durations of the order of the picosecond pulses which produced them, it became clear that these 'white' light pulses would be very useful for time-resolved spectroscopy. In figure 1, the H_2O cell in the path of the analysing beam is used to disperse the narrow-band probe pulse into a continuum.

Time dispersion

Dispersion of the probe pulse in time, in a manner which is experimentally resolvable, has taken two principal forms. The cross-beam technique (Malley & Rentzepis 1969, 1970) gives continuous dispersion but suffers from problems of intensity requirements and geometric optical complications and thus will not be discussed here. The echelon technique (Topp *et al.* 1971) provides discrete dispersion by creating a set of optical paths for different parts of the cross-sectional area of the probe beam, such that each optical path has a different transit time for light. Typically, the echelon takes the form of a stepped wedge made by a set of mirrors (reflexion echelon) or by a set of optically contacted glass or quartz plates (transmission echelon) which impress the time information along the cross section of the beam. The intersegment separation depends on the thickness of the glass plates and the angle of propagation. Typical delays are 2–5 ps for millimetre plate thickness, although several other echelons have been used with variable steps corresponding to interpulse separation varying from 5 to 100 ps, thus enabling one echelon to cover a 500 ps time range.

Time-resolved absorption spectra

After the wavelength and time-resolved dispersion are impressed upon each probe pulse, it is usually split into two identical portions (beam splitter B_4 in figure 1) to produce I and I_0 beams for dual-beam spectrometer operation (Netzel & Rentzepis 1974; Huppert *et al.* 1976). The I beam propagates through the sample irradiated by the excitation pulse, while the I_0 beam is passed through a reference cell containing solvent only, or in some cases through a sample which has not been irradiated by an excitation pulse (for difference spectroscopy). The two beams are then passed into a spectrograph with the time dispersion axis of the two beams resolved along the slit. At the output of the spectrograph a two dimensional image is recorded, which has the time dispersion resolved along one axis and wavelength resolved on the orthogonal axis. An example of such a two dimensional spectrum is shown in figure 3 and a simple plot of τ against transmission in figure 4.

Detection and data processing

The two dimensional images obtained with single pulse-time and wavelength resolved spectroscopy have been recorded in the past by using photographic techniques. Significant improvements have been made recently in the speed and convenience of data processing and in the sensitivity and linearity of optical signal recording by use of vidicon camera technology. Since the video data are collected directly in the form of electronic signals, the experimental results may be readily digitized for online computer processing.

Because the complete time and wavelength dependence is recorded with a single shot, the information content of the resulting two dimensional image can be extremely high. High-speed

PHILOSOPHICAL TRANSACTIONS OF THE ROYAL SOCIETY A MATHEMATICAL, PHYSICAL & ENGINEERING SCIENCES

computer processing and analysis greatly facilitate evaluation and compacting of data. An example of the types of compacted data display that are promptly available from direct computer analysis of images similar to that shown in figure 3 is presented in figure 5 (Huppert *et al.* 1977).

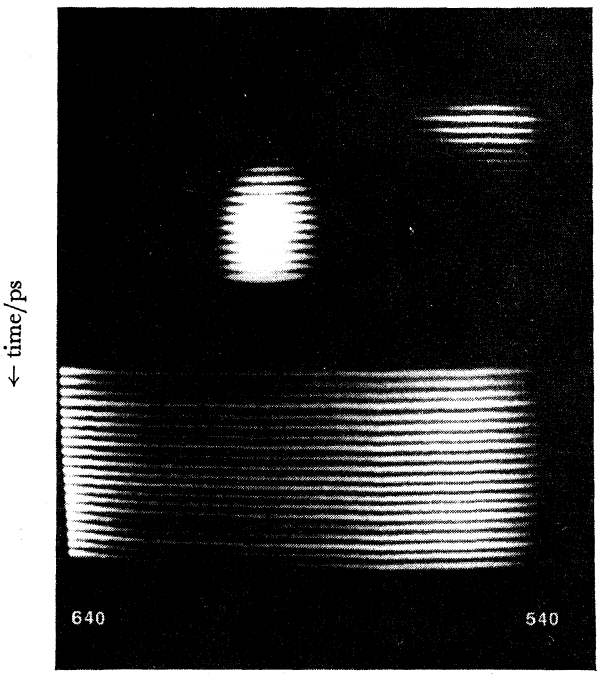

FIGURE 3. Picosecond time and wavelength resolved absorption spectrum displayed on a TV monitor. The reference spectrum (I_0) in the lower half of the figure, is used in conjunction with the upper spectrum (I) to calculate I_0/I. In the I spectrum, each horizontal bar is a full absorption spectrum which is separated in time from adjacent segments by 4 ps. These results pertain to energy transfer between malachite green and DODCI (Huppert *et al.* 1978).

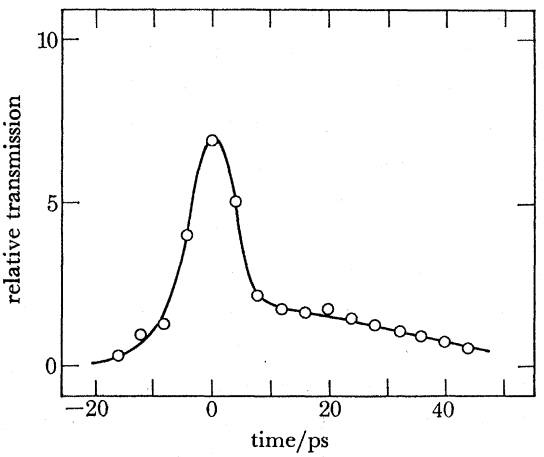

FIGURE 4. Picosecond time resolved bleaching of the triphenylmethane dye, crystal violet on methanol solution (2×10^{-4} M, 2 mm cell), excited by a 530 nm pulse and probed with 570 nm continuum light (Huppert *et al.* 1978).

PHILOSOPHICAL TRANSACTIONS OF THE ROYAL SOCIETY A MATHEMATICAL, PHYSICAL & ENGINEERING SCIENCES

Primary processes in rhodopsin

The initial studies on rhodopsin were performed before the development of wavelength continuum techniques, and exemplify the single-wavelength limitation; current investigation with the use of dispersive techniques, the continuum and the two-dimensional vidicon display, make it possible to observe the complete spectrum with a single shot. Previous stationary studies at low temperature have shown that the intermediate, prelumirhodopsin, is formed, first decaying into lumirhodopsin followed by the intermediates meta I and meta II (Yoshizawa & Kito 1958; Yoshizawa & Wald 1963; Yoshizawa 1972). The first intermediate, prelumirhodopsin, was identified at low temperatures; however, its physiological temperature kinetics were unknown because of its rapid formation and decay. Later transients were found to be *trans* isomers of the original *cis*-rhodopsin and therefore a number of workers (Rosenfeld *et al.* 1977) assumed that the initial action of light causes isomerization of the retinal and that the prelumirhodopsin intermediate is a *trans* isomer of rhodopsin.

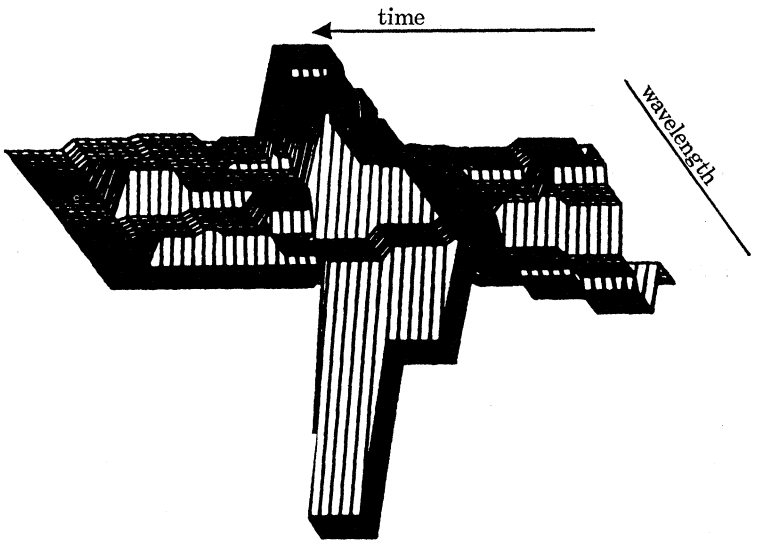

FIGURE 5. Simultaneous three dimensional display of time-dependent spectrum of reduced cytochrome *c* excited by a single 6 ps 530 nm pulse. The time element was provided by a stepped delay echelon and the spectral resolution by a spectrograph. The detection element was a vidicon whose output was analysed by a 1200 Nova computer.

The earliest species observed in the sequence, prelumirhodopsin, was unique among the intermediates in that it was the only one which had an absorption maximum shifted to the red (λ_{max} = 543 nm) of normal dark-adapted rhodopsin (λ_{max} = 500 nm). Thus by using a probe pulse at a Stokes Raman-shifted wavelength (561 nm) within the absorption band for prelumirhodopsin, it was possible to monitor its appearance and disappearance.

With this approach, an absorbing species was observed (Busch *et al.* 1972) which was interpreted to be prelumirhodopsin. The species appeared immediately upon excitation (within *ca.* 6 ps resolution of the experiment) and it decayed with a time constant of about 50 ns. This result provided strong evidence for the production of prelumirhodopsin at physiological temperatures and also permitted conclusions to be drawn concerning the types of structural changes that might be occurring in the molecule that would be consistent with this timescale.

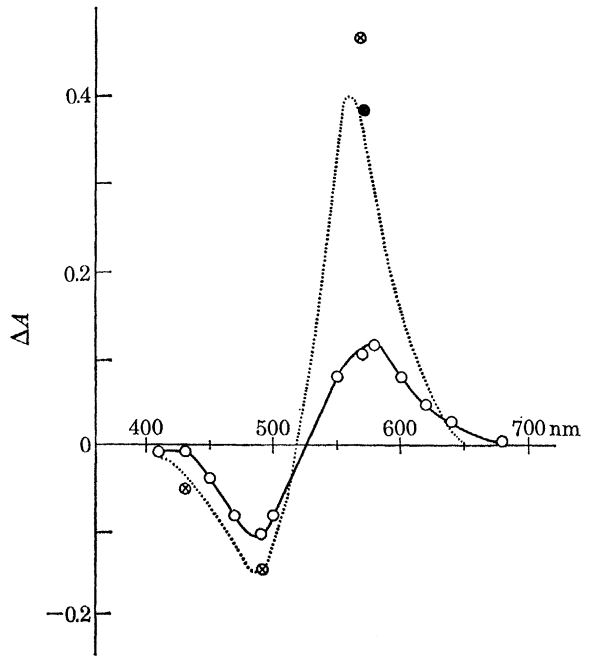

FIGURE 6. Prelumirhodopsin difference spectrum. ○, Recorded 298 K, 60 ps after excitation with a 5 mJ pulse at 530 nm (4); ●, 77 K and ⊗, 4 K; ·····; difference spectrum generated by photostationary studies of low-temperature glasses for 77 K (Bensasson *et al.* 1975) and 7 K (Grellman *et al.* 1962; Tokunaga *et al.* 1976). Photostationary studies at 77 K and 7 K give identical difference spectra. The data are normalized to concentrations used for this kinetic study. Rhodopsin was solubilized in 0.3 M Ammonyx/0.01 M Hepes at pH 7.0; $A_{500} = 0.73$ in 2 mm.

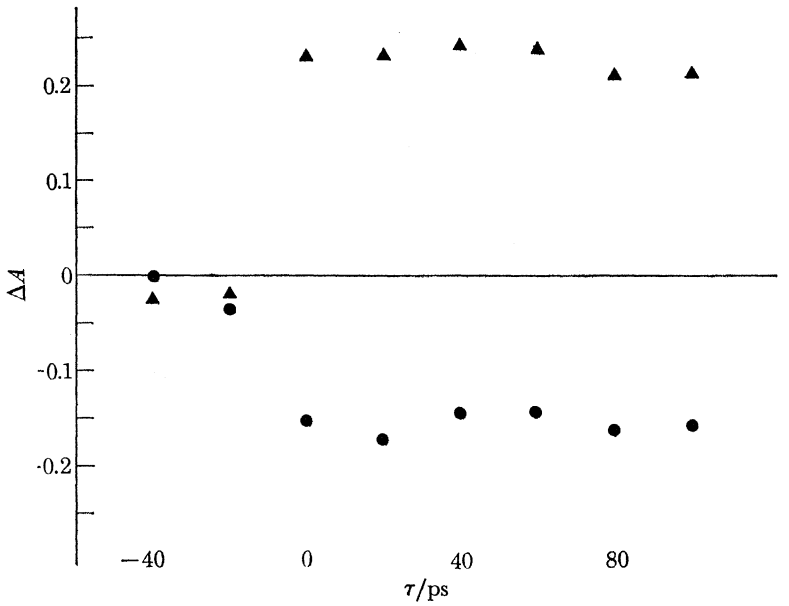

FIGURE 7. (*a*) Formation of the prelumirhodopsin band with a maximum at 580 nm induced by a 530 nm 6 ps pulse; ▲, 580 nm; ●, 480 nm. (*b*) Depletion rate of the rhodopsin band at 480 nm after excitation with the 530 nm pulse. Similar kinetics are observed over the entire spectrum of these two bands. Both curves represent the average of five repeated runs.

PHILOSOPHICAL TRANSACTIONS OF THE ROYAL SOCIETY A MATHEMATICAL, PHYSICAL & ENGINEERING SCIENCES

To verify that indeed this absorption monitored (Busch *et al.* 1972) at 560 nm corresponds to prelumirhodopsin, the complete difference spectra for prelumirhodopsin at room temperature at various time delays after 530 nm excitation were measured in the time range 6–300 ps (Sundstrom *et al.* 1977). The difference spectra (figure 6) thus obtained showed (1) the bleached rhodopsin band between 430 and 510 nm with a maximum ΔA at 485 nm, and (2) the formation of a band at 530–680 nm with a maximum at 580 nm. An approximate isobestic point is visible at 525 nm; this difference spectrum is in good agreement with the previously reported low-temperature spectrum. The rhodopsin bleached within 6 ps and the prelumirhodopsin band was formed also within 6 ps (figure 7*a*, *b*). Since the formation time of prelumirhodopsin at room temperature is faster than the time width of the pulse, lower-temperature observations of the formation of prelumirhodopsin were needed for the elucidation of this process. Such

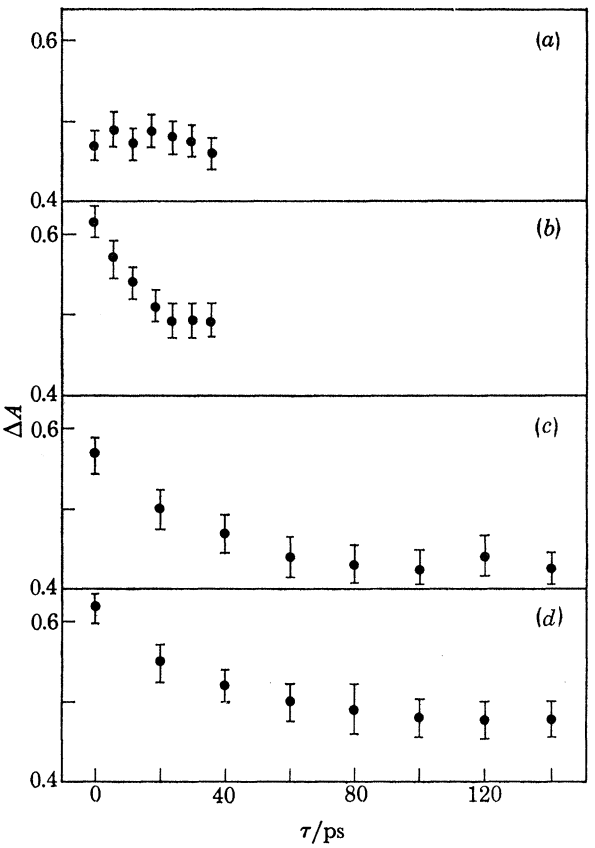

FIGURE 8

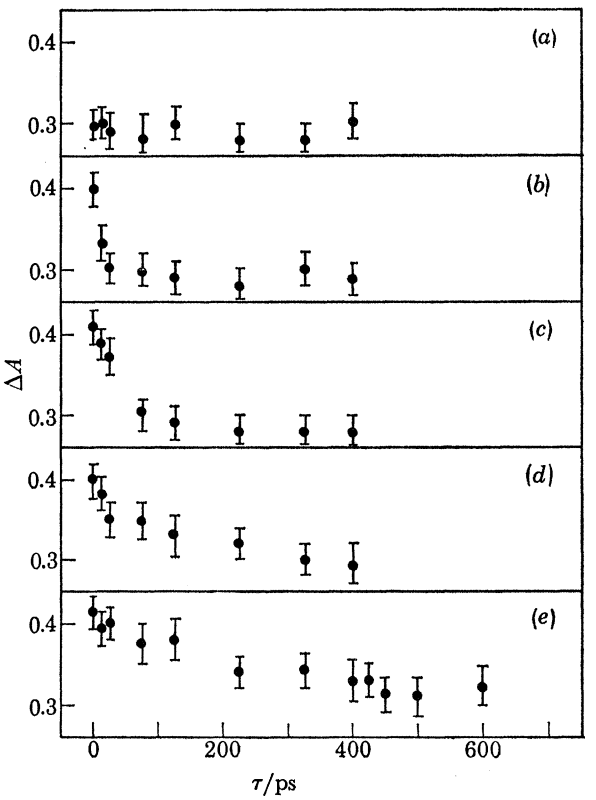

FIGURE 9

FIGURE 8. Kinetics of formation of prelumirhodopsin at various temperatures monitored at 570 nm. Excitation of rhodopsin was with a 5 mJ, 530 nm, 6 ps pulse. The glass for low temperature study was formed by mixing 1 part rhodopsin, solubilized in 0.3 M Ammonyx/0.01 M Hepes at pH 7.0, $A_{500} = 10.0$, with 2 parts distilled ethylene glycol. The lifetime for formation, given in the upper right of each panel, is the reciprocal of the rate constant obtained by a least square fit of $\ln (A_t - A_\infty)$ against time, t, in which A is absorbance at 570 nm. (*a*) 30 K, 6 ps; (*b*) 20 K; 9 ± 2 ps; (*c*) 10 K, 29 ± 2 ps; (*d*) 4 K, 36 ± 2 ps. The variance is designated by the error bars.

FIGURE 9. The kinetics of formation of deuterium-exchanged prelumirhodopsin at various wavelengths. The excitation of deuterium-exchanged rhodopsin was with a 5 mJ, 530 nm, 6 ps pulse. The glass for low temperature study was formed by mixing 1 part D-rhodopsin in deuterium-exchanged 0.1 M Ammonyx/0.01 M Hepes at pH 7.0, $A_{500} = 7.0$, with 2 parts deuterium exchanged ethylene glycol. The lifetime of formation was calculated as for figure 8. (*a*) 50 K, 6 ps; (*b*) 40 K, 17 ± 2 ps; (*c*) 30 K, 51 ± 5 ps; (*d*) 20 K, 175 ± 13 ps; (*e*) 4 K, 257 ± 28 ps.

PHILOSOPHICAL TRANSACTIONS OF THE ROYAL SOCIETY A MATHEMATICAL, PHYSICAL & ENGINEERING SCIENCES

experiments between 300 and 4 K reveal that, as low as 77 K, the rise-time of the band at 570 nm is still less than 10 ps and only below 30 K could finite rise-times be observed (Peters *et al.* 1977). Even at 4 K the rise-time was only 36 ps as shown in figure 8.

To elucidate these data, which are not expected if one is to assume that the isomerization mechanism is responsible for the formation of prelumirhodopsin at low temperatures, the rhodopsin was immersed in D_2O, thus allowing the substitution of all exchangable protons with deuterium. It is well known that the hydrogens of the retinal chromophore do not exchange except for the proton of the protonated Schiff base which easily exchanges for deuterium in D_2O (Oseroff & Callender 1974). The rationale for the deuterated experiment was that if isomerization of the retinal is responsible for the observed kinetics, then deuterium substitution will not cause a major change in the rates since the retinal protons remain intact.

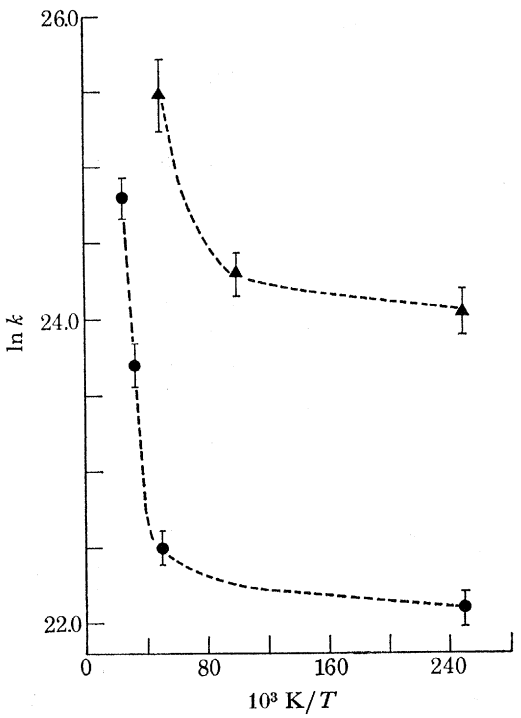

FIGURE 10. An Arrhenius plot, ln k for formation of prelumirhodopsin against T^{-1}, of the kinetic data in figures 8 and 9. The value ln k = 25.84 corresponds to a lifetime of 6 ps, our minimal time resolution. ▲, rhodopsin; ●, D-rhodopsin.

For the deuterated rhodopsin it was observed that the rates for the formation of prelumirhodopsin were much slower than its protonated homologue. Measured at 570 nm, D-rhodopsin samples show that at 40 K the rate of formation of prelumirhodopsin is 17 ps without any subsequent decay. As the temperature decreases the rate was found to have values ranging from 51 ps at 30 K to 256 ps at 4 K (figure 9) which is to be contrasted with the H-rhodopsin formation lifetimes of 9 ps at 30 K to 36 ps at 4 K (figure 8).

A transient species is also observed which decays fast into a long-lived species absorbing at 570 nm. We believe that this is an excited singlet state of rhodopsin prepared by the 530 nm excitation pulse, assuming a vibrationally relaxed system and trivial local heating as a result of vibrational relaxation.

Proton translocation

The photoinduced process which converts rhodopsin into prelumirhodopsin via the excited state appears to be very efficient as no significant rhodopsin ground state repopulation is observed during the first 100 ps after excitation. Information concerning the nature of the photo-induced process responsible for the bleaching of rhodopsin at these lower temperatures and formation of prelumirhodopsin can be obtained by a closer examination of the temperature dependence of the formation rate constant K_{pl} of prelumirhodopsin and its isotope dependence. Figure 10 shows the temperature dependence of K_{pl} plotted in the Arrhenius form ($\ln K$ against T^{-1}). Two striking features of this plot are immediately apparent: (1) The plot of $\ln K_{pl}$ against T^{-1} is not linear as expected for an Arrhenius process. (2) As $T \to 0$ the rate constant K_{pl} becomes temperature independent, reaching a non-zero constant which is not expected for a process governed by Arrhenius kinetics.

Considering the effect of deuteration on K_{pl}, we see that the rate is slower at low T^{-1} in the deuterated rhodopsin, the ratio K_{pl}^{H}/K_{pl}^{D} being approximately 7. As the proton of the protonated Schiff base is an exchangable one in the retinal sequence, in the absence of drastic changes of the protein structure caused by the D_2O, the observed isotope dependence suggests specific effects similar to that found in excited-state proton transfer reactions (Ingham & El Bayoumi 1974; Avouris *et al.* 1976). The nonlinear Arrhenius plot and the constant low-temperature value of K_{pl} strongly suggest a tunnelling process (Löwdin 1965). Because of the strong dependence of the tunnelling rate on the mass of the tunnelling particle, only light particles such as electrons and protons are expected to tunnel efficiently. Proton tunnelling has indeed been proposed to take place in some excited-state proton transfer reactions (Avouris *et al.* 1976, Löwdin 1965). The results for temperature and isotope dependence strongly suggest a proton-transfer reaction as being mainly responsible for the formation of prelumirhodopsin at low temperatures. There are several other results that also support the proton-transfer mechanism. The absorption spectrum of prelumirhodopsin is red-shifted with respect to the spectrum of rhodopsin itself, and therefore prelumirhodopsin may be a more tightly protonated Schiff base than rhodopsin. Model studies (Waddell & Becker 1971) indicate that translocating the proton towards the Schiff base nitrogen could account for the spectral red shift.

The mechanism of formation of prelumirhodopsin at higher temperatures has been described as a *cis-trans* isomerization. The extremely fast formation of prelumirhodopsin at 4 K, though, argues against such an isomerization process at these low temperatures. Several studies, for example, had shown (Waddell *et al.* 1973) that as the temperature is decreased, the quantum yield of photo-isomerization of retinal analogues and retinal Schiff bases decreases, and at 77 K photoisomerization does not take place at all. Analogous results were also found for the isomerization of stilbene (Saltiel *et al.* 1973). On the other hand, the mechanism of the formation of prelumirhodopsin at higher temperatures cannot be ascertained from the available results. Regarding the mechanism for the proton translocation process, existing theories are not sufficiently refined to give an exact answer. However, assuming that the expression (Löwdin 1965)

$$\kappa_t = \nu_0 \exp\left[(-\pi^2 a_0 K/h)\,(2ME)^{\frac{1}{2}}\right] \qquad (1)$$

is applicable for the case of rhodopsin we can calculate an activation energy or barrier height, E_a (figure 7), and a width of the barrier or translocation distance a_0. By using the

PHILOSOPHICAL TRANSACTIONS OF THE ROYAL SOCIETY A MATHEMATICAL, PHYSICAL & ENGINEERING SCIENCES

experimental rate constant of 2.8×10^{11} s^{-1} at 4 K, and the normal value for Planck's constant h, and the mass of the proton M, we calculate an E_a value of 5.85 kJ mol^{-1} if we assume that ν_0 takes the value of the N—H band frequency of 1500 cm^{-1}. If we use instead the more reasonable value of 10^{13} for the frequency of the translocated proton, we calculate a barrier of 3.1 kJ mol^{-1} or a height of *ca.* 0.6 kJ mol^{-1} above room RT. This indicates that at room temperature the proton translocation could be an activated process proceeding without a barrier, and would explain the ultrafast rate observed for the formation of prelumirhodopsin at room temperature. Similarly, the distance, a_0 through which the proton tunnels, is calculated to be *ca.* 0.5 Å.†

Models for proton tunnelling

The kinetic data presented originally by Peters *et al.* (1977) have been found to be consistent with at least two mechanisms leading to the formation of prelumirhodopsin. These are (1) a concerted double-hydrogen transfer leading to a retro-retinal structure, which is a slightly different mechanism from the one proposed previously (von der Maer *et al.* 1976); (2) a single-proton translocation to the Schiff base nitrogen generating a carbonium ion as proposed previously by Salem & Bruckmann (1975), Salem (1976) or Maties & Stryer (1976). The proton translocation is thought to be facilitated by an active role of an amino acid with histidine being a strong candidate (figure 11). At present, we can postulate several other candidates and mechanisms involving the proton; however, until more definitive evidence is available we shall limit our proposals to the above two models represented schematically in figure 8. Examining further the histidine hypothesis, we believe that, should this be the case, translocation would occur between the hydrogen-bonded nitrogens of the histidine and Schiff base and the hydrogen would translocate along the N—H stretch coordinate toward the Schiff base nitrogen which is proposed to have a 'negative' character in the excited state, thus providing the force for the proton translocation. Assuming that the proton is originally shared by the two nitrogens $N_h \cdots H \cdots N_S$, the translocation distance will be *ca* 0.5 Å, while if held strongly by the histidine nitrogen N_h—$H \cdots N_S$, then the distance for translocation would be *ca.* 0.9 Å (N_h is the histidine nitrogen, N_S is the Schiff base nitrogen). In the case of the single proton translocation, the carbonium ion would be relatively long-lived and no need for immediate stabilization would be necessary. In the two proton model one can envisage stabilization by the removal of a hydrogen from an adjacent carbon. Protein conformational changes would be affected by the proton translocation; however, the magnitude of change and the rate with which they occur, especially at these low temperatures, are not thought to be high. At the present time one can only conclude from the data that tunnelling is the dominant mechanism in the formation of prelumirhodopsin at low temperatures. The isotope exchange D for H strongly supports our tunnelling proposal and shows that proton tunnelling indeed takes place. The present data do not provide an unequivocal distinction between the protons.

Summary

Picosecond spectroscopy allows one to detect and measure, with considerably accuracy, processes which take place in the picosecond range. The data can be recorded and displayed automatically in the form of a three dimensional plot of time (picosecond resolution), wavelength (3 cm^{-1} resolution or less) and change in optical density (reproducibility of 0.02 and

† 1 Å = 10^{-10} m = 10^{-1} nm.

much lower sensitivity). Such a method has permitted study of several processes from azulene vibrational relaxation to intersystem crossing in benzophenone, to electron dynamics and to the primary events in [bacterio]chlorophyll and vision. New information has been obtained in all these cases, and mechanisms such as the proton tunnelling in rhodopsin, discussed in some detail here, have been proposed as a result of the data made possible by picosecond spectroscopy.

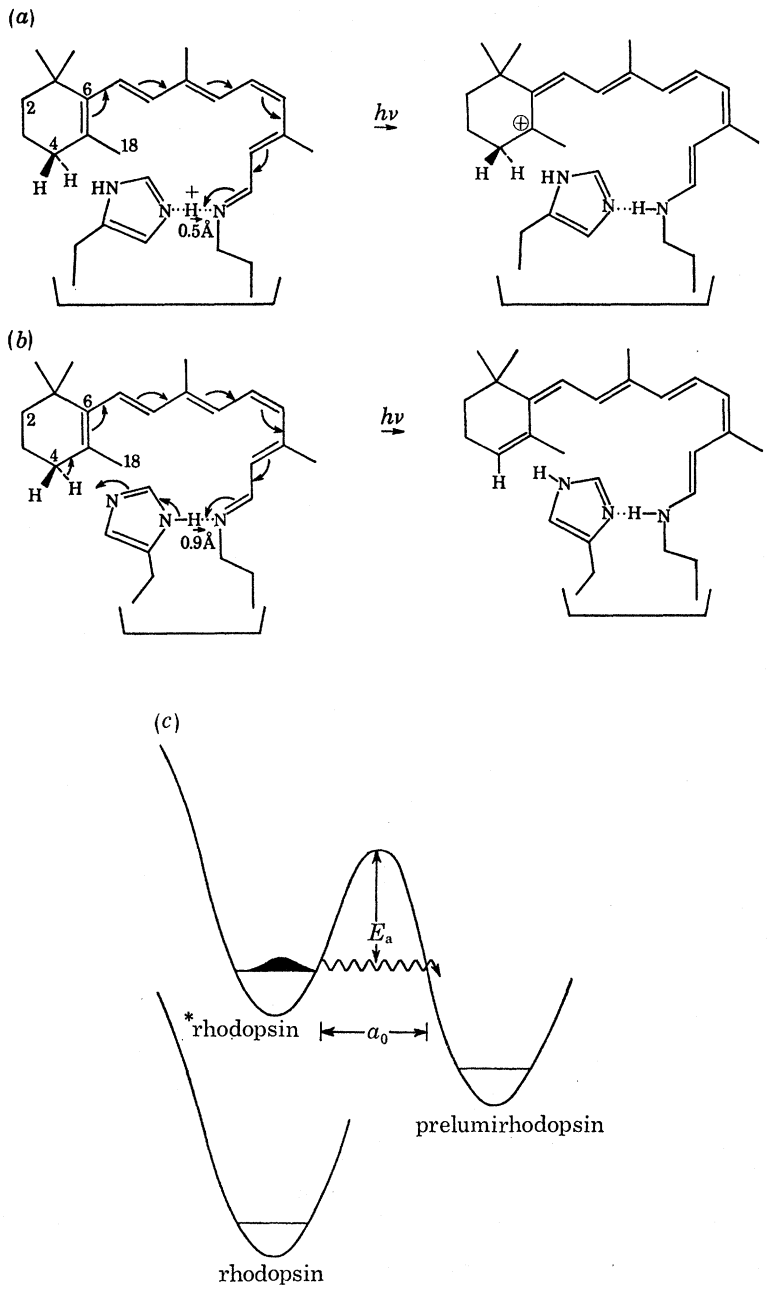

FIGURE 11. Models for proton translocation to form prelumirhodopsin; model (*a*) single proton translocation with carbonium formation; model (*b*) concerted double proton translocation with retro-retinal formation. The tunnelling distances, a_0, through the barriers for the formation of prelumirhodopsin are 0.5 Å for single proton model (*a*) and 0.9 Å for the concerted double proton translocation.

Most of the work described on the various techniques was done in collaboration with Dr G. E. Busch (K.M.S.), Dr T. L. Netzel (Brookhaven), Professor W. S. Struve (Iowa State University), Professor K. J. Kaufmann (University of Illinois). Dr K. S. Peters (Harvard University), Dr V. Sundstrom (Umea University), Professor M. L. Applebury was the principal force in the vision studies. To the above and to Dr D. C. Douglass I am most grateful.

References (Rentzepis)

Alfano, R. R. & Shapiro, S. L. 1970 *Phys. Rev. Lett.* **24**, 584.
Alfano, R. R. & Shapiro, S. L. 1975 *Physics Today* p. 30.
Avouris, P., Yang, L. L. & El Bayoumi, M. A. 1976 *Photochem. Photobiol.* **24**, 211.
Beens, H., Grellmann, K. H. & Weller, A. H. 1965 *Discuss. Faraday Soc.* **39**, 183.
Bensasson, R., Land, E. J. & Truscott, T. G. 1975 *Nature, Lond.* **285**, 708.
Bradley, D. J. & Siebert, W. 1973 *Opt. Commun.* **9**, 17.
Busch, G. E., Applebury, M. L., Lamola, A. A. & Rentzepis, P. M. 1972 *Proc. natn. Acad. Sci., U.S.A.* **69**, 2802.
Busch, G. E., Jones, R. P. & Rentzepis, P. M. 1973 *Chem. Phys. Lett.* **18**, 178.
Chiao, R. & Stoicheff, B. P. 1964 *Phys. Rev. Lett.* **12**, 290.
Colles, M. J. 1969 *Opt. Commun.* **1**, 169.
Eisenthal, K. B. 1975 *Accts Chem. Res.* **8**, 118.
Glenn, W. H. & Brienza, M. J. 1967 *Appl. Phys. Lett.* **10**, 221.
Grellman, K. H., Livingston, R. & Pratt, D. 1962 *Nature, Lond.* **193**, 1258.
Gustafson, T. K., Taran, J. P., Haus, H. A., Lifshitz, J. R. & Kelley, P. L. 1969 *Phys. Rev.* **177**, 306.
Huppert, D. & Rentzepis, P. M. 1976 *Molecular energy transfer* (ed. R. Levine & J. Jortner), pp. 270–279. New York: John Wiley and Sons.
Huppert, D. & Rentzepis, P. M. 1978 *J. appl. Phys.* **49**, 543.
Huppert, D., Struve, W. S., Rentzepis, P. M. & Jortner, J. 1975 *J. chem. Phys.* **63**, 1205.
Huppert, D., Straub, K. D. & Rentzepis, P. M. 1977 *Proc. natn. Acad. Sci., U.S.A.* **74**, 4139.
Huppert, D., Busch, G. E. & Rentzepis, P. M. 1978 *Opt. Engng* **17**, 82.
Ingham, K. C. & El Bayoumi, M. A. 1974 *J. Am. chem. Soc.* **96**, 1674.
Kaufmann, K. J. & Rentzepis, P. M. 1975 *Accts chem. Res.* **8**, 407.
Laubereau, A. & Kaiser, W. 1975 *A. Rev. phys. Chem.* **26**, 83.
Löwdin, P.-O. 1965 *Adv. Quantum Chem.* **2**, 213.
Malley, M. M. & Rentzepis, P. M. 1969 *Chem. Phys. Lett.* **3**, 534.
Malley, M. M. & Rentzepis, P. M. 1970 *Chem. Phys. Lett.* **7**, 57.
Mathies, R. & Stryer, L. 1976 *Proc. natn. Acad. Sci., U.S.A.* **73**, 2169 (1976).
Netzel, T. L. & Rentzepis, P. M. 1974 *Chem. Phys. Lett.* **24**, 337.
Oseroff, A. & Callender, R. 1974 *Biochemistry* **13**, 4243.
Peters, K., Applebury, M. L. & Rentzepis, P. M. 1977 *Proc. natn. Acad. Sci., U.S.A.* **74**, 3119.
Rentzepis, P. M. 1968 *Chem. Phys. Lett.* **2**, 117.
Rosenfeld, T., Honig, B., Ottolenghi, M. & Ebrey, T. G. 1977 *Pure appl. Chem.* **49**, 341.
Salem, L. 1976 *Science, N.Y.* **191**, 822.
Salem, L. & Bruckmann, P. 1975 *Nature, Lond.* **258**, 526.
Saltiel, J., D'Agostino, J., Megarity, E. D., Metts, L., Nearberger, K. R., Wrighton, M. & Zafiriou, O. I. 1973 *Organic Photochem.* **3**, 1.
Shimizu, F. 1967 *Phys. Rev. Lett.* **19**, 1097.
Sundstrom, V., Rentzepis, P. M., Peters, K. S. & Applebury, M. L. 1977 *Nature, Lond.* **267**, 645.
Tokunga, R., Kawamura, S. & Yoshizawa, T. 1976 *Vision Res.* **16**, 633.
Topp, M. R., Rentzepis, P. M. & Jones, R. P. 1971 *J. appl. Phys.* **42**, 3451.
von der Meer, K., Mulder, J. J. C. & Lugstenburg, J. 1976 *Photochem. Photobiol.* **24**, 363.
von der Linde, D. 1972 *IEEE J. Quantum Electron* QE-8, 328.
Waddell, W. & Becker, R. S. 1971 *J. Am. chem. Soc.* **93**, 3788.
Waddell, W., Schaeffer, A. M. & Becker, R. S. 1973 *J. Am. chem. Soc.* **95**, 8233.
Yoshizawa, T. 1972 *Handbook of sensory physiology* (ed. H. Dortnell), vol. VII/I, pp. 146–179. Berlin: Springer–Verlag.
Yoshizawa, T. & Kito, Y. 1958 *Nature, Lond.* **182**, 1604.
Yoshizawa, T. & Wald, G. 1963 *Nature, Lond.* **197**, 1279.

PHILOSOPHICAL TRANSACTIONS OF THE ROYAL SOCIETY A MATHEMATICAL, PHYSICAL & ENGINEERING SCIENCES

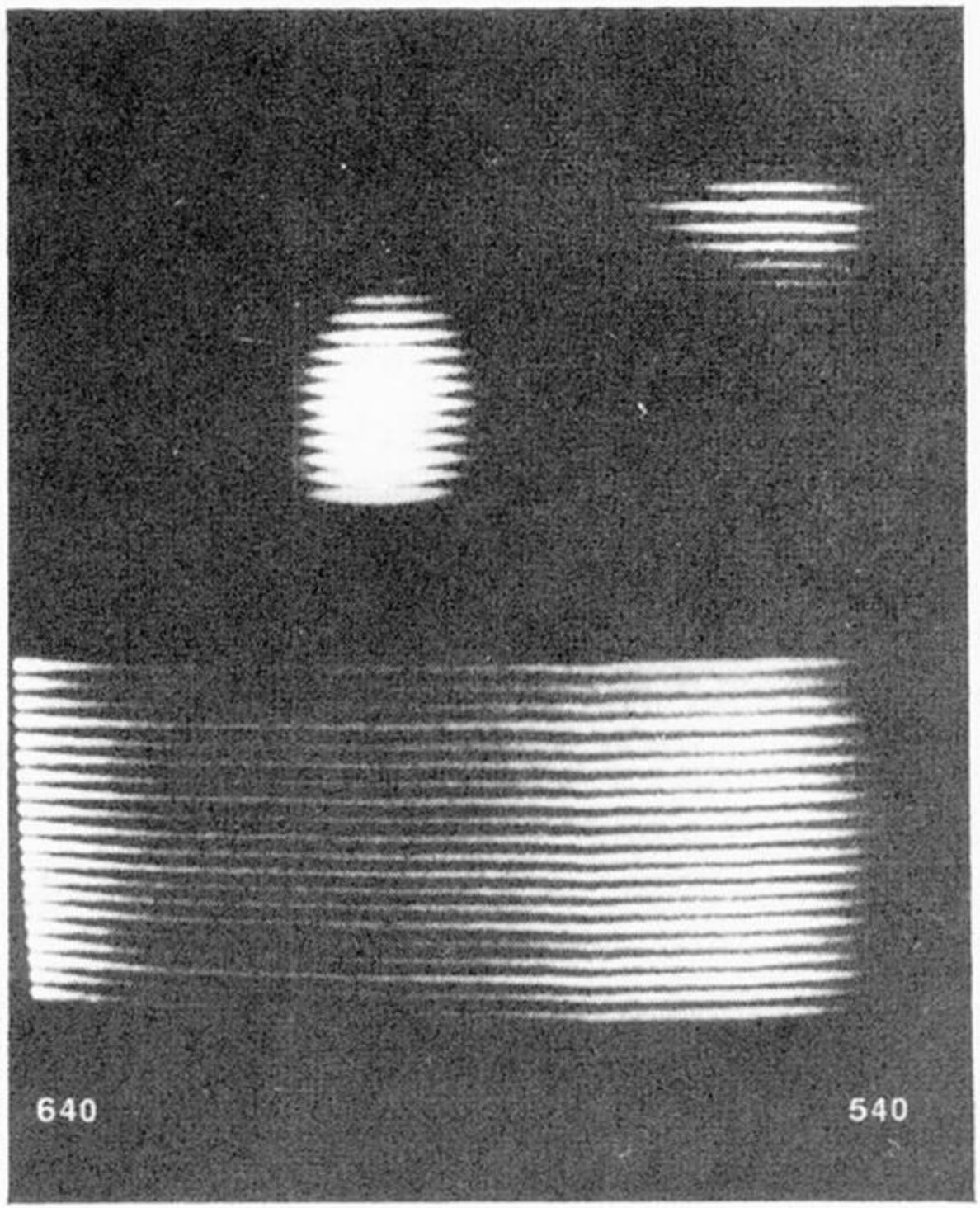

FIGURE 3. Picosecond time and wavelength resolved absorption spectrum displayed on a TV monitor. The reference spectrum (I_0) in the lower half of the figure, is used in conjunction with the upper spectrum (I) to calculate I_0/I. In the I spectrum, each horizontal bar is a full absorption spectrum which is separated in time from adjacent segments by 4 ps. These results pertain to energy transfer between malachite green and DODCI (Huppert *et al.* 1978).